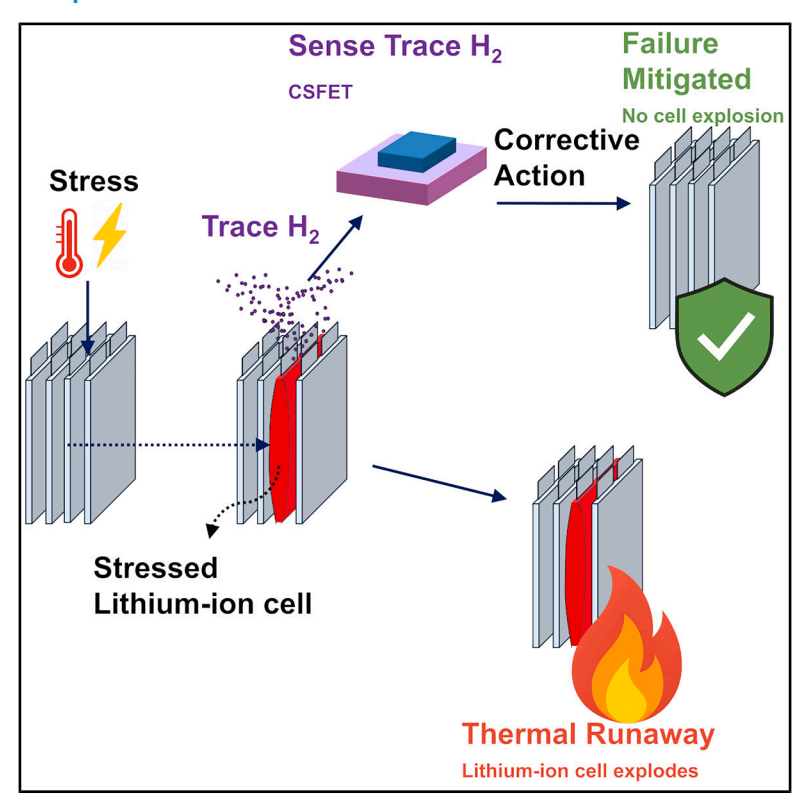
Cell Reports Physical Science

Mitigating lithium-ion cell thermal runaway via selective trace H₂ sensing

Graphical abstract



Authors

David W. Gardner, Gordon Charles, Thach Nguyen, Ali Javey, Hossain M. Fahad

Correspondence

fahad@serinuslabs.com

In brief

Gardner et al. report that selective trace hydrogen sensing with chemically sensitive field-effect transistors provides early and reliable warning of lithium-ion cell thermal runaway across diverse cathode chemistries and stress modes. Timely intervention upon hydrogen detection mitigates cell-level failure, supporting a broadly applicable and scalable safety solution.

Highlights

- Trace hydrogen sensors provide early warning of lithium-ion cell thermal runaway
- Trace hydrogen sensors outperform temperature, voltage, and pressure monitoring
- Early intervention guided by trace hydrogen detection prevents thermal runaway
- Tested across NCA, NMC, and LFP cathode chemistries at all states of charge





Cell Reports Physical Science



Article

Mitigating lithium-ion cell thermal runaway via selective trace H₂ sensing

David W. Gardner, 1,3 Gordon Charles, 1,3 Thach Nguyen, 1 Ali Javey, 2 and Hossain M. Fahad 1,4,*

SUMMARY

Thermal runaway in lithium-ion batteries poses a major safety risk. Prior to thermal runaway, cells vent their internal gases as the internal pressure rises, with hydrogen detectable at trace levels of tens to hundreds parts per million. Here, we report that selective trace hydrogen detection, using chemically sensitive field-effect transistors, provides reliable early warning of imminent thermal runaway across multiple cell types and abuse conditions. Systematic abuse tests on commercial cylindrical nickel-cobalt-aluminum (NCA) cathode, pouch nickel-magnanese-cobalt (NMC) cathode, and prismatic lithium-iron-phosphate (LFP) cathode cells at 10%–100% state of charge show that hydrogen is consistently detected in vented gases before thermal runaway. Trace hydrogen detection proves more reliable than conventional temperature, voltage, and pressure sensors. When cell abuse is stopped upon early hydrogen detection, thermal runaway is successfully prevented in all tested cases. These findings establish that trace hydrogen sensing provides early, actionable intelligence to prevent thermal runaway.

INTRODUCTION

The major safety concern with lithium-ion cells is the possibility of thermal runaway 1-4 (Figure 1). Lithium-ion cells stressed by high temperature, overcharging, mechanical deformation, or defects can develop internal exothermic chemical reactions, causing the cell temperature to rise, 1.5-11 degrading the cell components. The internal pressure of the cell increases until the cell housing fails in a first venting event. If no action is taken, then the cell temperature continues to rise until the cell explodes. The explosion can spread to other cells as thermal runaway propagation in an extremely dangerous cascade. Aged cells 12.13 and cells at higher states of charge 6.14,15 are more vulnerable to thermal runaway propagation.

The thermal runaway problem is particularly significant in the automotive domain due to the growing demand for electric vehicles. To ensure safety, regulatory frameworks are instigating new mandates related to lithium-ion batteries to warn occupants prior to thermal runaway propagation. 16,17

Existing battery health monitoring sensors are incapable of providing sufficient prognostic capability to avert cell thermal runaway. Specifically, voltage and current sensing are limited where the cells are in parallel and series configurations. Temperature sensors are only effective if each cell has a sensor, which is an impractical implementation. Therefore, robust prognostics are needed to detect when a single cell is in danger of entering thermal runaway.

Gas sensors to detect the first venting event are gaining attention 18-24 because a first venting event is a nearly ubiquitous feature of lithium-ion cells that will eventually enter thermal runaway. This is especially beneficial in cases of latent failures due to cell abuse over time, which is non-trivial to diagnose with existing sensors. However, gas detection may not detect every type of failure, especially in cases where there is minimal time between a venting event and thermal runaway.

The first venting gases are primarily CO_2 , CO, C_2H_4 , battery electrolytes, and hydrogen. ^{25–27} Hydrogen is an attractive target for cell venting detection because (1) it is distinctive to cell venting, not existing in the atmosphere, so there are few false positives; (2) it is a fundamental gas generated by a wide variety of battery chemistries; and (3) it has a high diffusion coefficient relative to other gases.

The main drawback of hydrogen is its lower relative concentration compared to other vented species. Commercially available hydrogen sensors based on thermal conductivity typically have detection limits of thousands of parts per million and could report "no hydrogen" following a venting event. However, when more sensitive tools are used, hydrogen is invariably detected.²⁰

Hydrogen can be generated in several ways. The simplest is electrolysis of trace water or water generated from electrolyte decomposition. A second is the reaction between lithium dendrites and polyvinylidene fluoride. A third is from solvent decomposition. 5,27,32–36

Xueqin and Lei³⁷ used graphite-graphite symmetric cells to show that hydrogen is generated irrespective of cathode



¹Serinus Labs, Inc., Berkeley, CA 94704, USA

²Electrical Engineering and Computer Sciences, University of California, Berkeley, Berkeley, CA 94720, USA

³These authors contributed equally

⁴Lead contact

^{*}Correspondence: fahad@serinuslabs.com https://doi.org/10.1016/j.xcrp.2025.102859



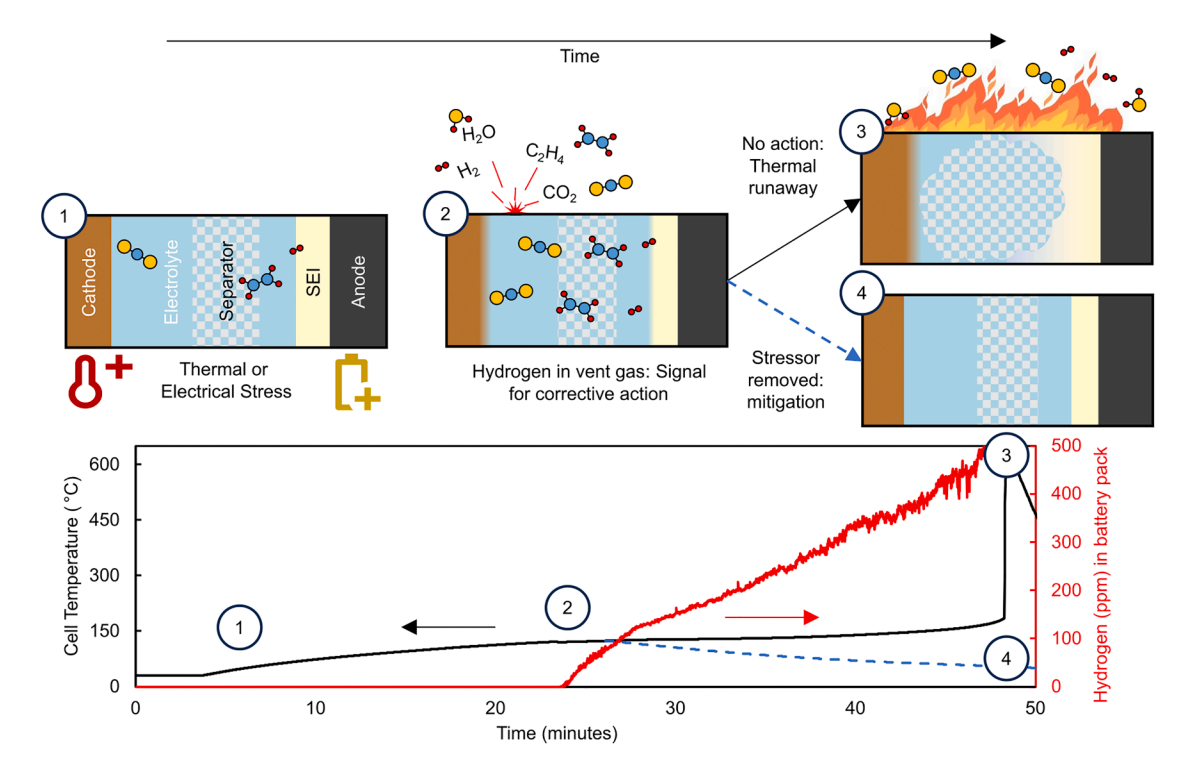


Figure 1. Lithium ion cell journey to thermal runaway

Top: evolution of cell temperature and battery pack hydrogen concentration for lithium-ion cells under stress. (1) Chemical reactions in the cell increase its internal pressure. (2) The cell vents. Various molecules are present in the plume. (3) If no action is taken, then the cell enters thermal runaway. (4) Hydrogen from the vented gas can be used to initiate cell cooling, mitigating thermal runaway.

material, supporting the notion that electrolyte fragments are generating hydrogen at the anode.³⁸ There are mixed reports on the effect of state of charge (SoC) on hydrogen content in stressed cells; Geng et al.³⁹ found that higher-SoC cells have more vented hydrogen, while others found no dependence.^{6,40}

Once hydrogen is vented, it must be detected. Several studies show that a limit of detection of approximately 100 ppm would be adequate to detect hydrogen in the first venting gas in a commercial stationary storage cabin. ^{18,21,22} In an automotive battery pack, such a sensor would be integrated with the battery management system to initiate a safety routine.

A hydrogen sensor for detecting lithium-ion cell venting should have the following characteristics: (1) a detection limit lower than 100 ppm, as described above; (2) low operating power consumption to prevent parasitic drain on the primary battery during the key-off state; (3) virtually no false positives to gases that may become present in an automotive atmosphere (e.g., CO_2 , CO, and hydrocarbons); and (4) a sensor lifetime greater than that of the battery pack for consumer safety. 4,10,23,25

In this study, a hydrogen chemically sensitive field-effect transistor^{41,42} (H₂-CSFET; Figure 2) selectively detects trace hydrogen vented from automotive lithium-ion cells prior to thermal runaway. We test the sensors in two thermal runaway scenarios: overheating and overcharging at 1 C. During these accelerated tests, hydrogen detection provides

24 min and 3.6 min of early warning, respectively, before thermal runaway. We then show that thermal runaway can be prevented by intervening after hydrogen detection across a variety of cell types and conditions: overheated cylindrical nickel-cobalt-aluminum (NCA)-cathode cells at 10%-100% state of charge, overheated pouch nickel-manganese-cobalt (NMC) cathode cells at 10%-100% state of charge; an overheated prismatic lithium-iron-phosphate (LFP) cathode cell at 100% state of charge; and an overcharged NMC pouch cell. Other sensing modalities monitor the cells, including voltage, cell case temperature, and ambient pressure. Only hydrogen detection reliably indicates cell venting. These results demonstrate that hydrogen sensing enables early detection and prevention of thermal runaway across lithium-ion cell formats, chemistries, states of charge, and abuse conditions. The reliable and broadly applicable hydrogen warning signal suggests that this approach could significantly enhance battery safety if integrated with battery management systems.

RESULTS

Venting prior to thermal runaway

Figure 3 shows the hydrogen concentration, measured voltage, and cell case temperature for two cases of thermal runaway: overheating of a cylindrical cell and overcharging of a pouch



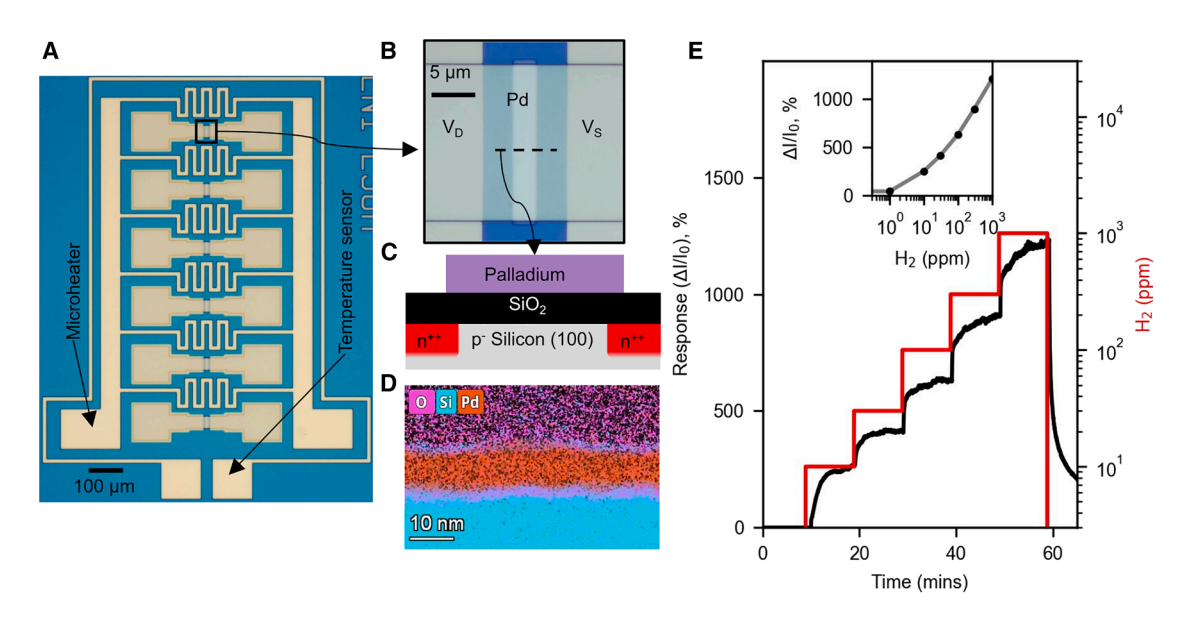


Figure 2. Overview of the H2-CSFET sensor

(A) Optical image of the sensor array. The inset shows the catalyst slab spanning the FET channel. Only one sensor from the array is used for a single measurement. Scale bar: 100 μm.

- (B) Optical image of a single sensor, showing the drain terminal, Pd thin film, and source terminal. Scale bar: 5 µm.
- (C) Cross-section of the dashed line in (B), showing the FET structure with a floating palladium thin-film sensing layer.
- (D) TEM EDS cross-section of the dashed line in (B), showing the catalyst thin film. Scale bar: 10 nm.
- (E) Normalized drain current during hydrogen exposure. The inset shows the drain current response to hydrogen. Limit of detection is <1 ppm.

cell. More detailed plots of each test are shown in Figures S7–S10 and Videos S1 and S2.

Overheating cylindrical cell

The cell temperature increased at approximately 6°C/min during heating. The cell vented when the case temperature reached 121°C. The measured voltage did not change at the venting event, and the pressure sensor did not detect the venting (<0.1 hPa).

After cell venting, the apparent heating efficiency decreased as the cell shed heat through its evaporating electrolyte, as seen in video frame 3 in Figure 3A. The hydrogen concentration in the abuse chamber continued to increase following the venting event. Approximately 30 min into the test, the internal cell reactions became self-sustaining, causing the cell case temperature's rate of rise to increase. The cell entered thermal runaway 23.9 min after the initial hydrogen signature was detected. The cell in parallel with the heated cell did not enter thermal runaway.

Overcharging pouch cell

During 1 C overcharging from 100% SoC, the pouch cell's case temperature increased very slowly until the first venting occurred. At venting, the cell case temperature was only 51°C, much lower than in the overheating test. Following venting, the temperature suddenly increased at a rate of approximately 13°C/min. The cell voltage dropped approximately 30 s after venting, and the pressure sensor detected a 0.4 hPa spike. The first venting coincided with the discontinuity in case temperature measurement. Video footage shows an increasing amount of smoke emanating from the cell after the first venting until thermal runaway occurred 3.6 min later. On thermal runaway, the resistance temperature detector (RTD) signal was lost.

In both cases, the vented hydrogen provided early warning compared to other cell sensing modalities. The next set of experiments will demonstrate that this information is actionable to mitigate thermal runaway.

Thermal runaway mitigation

The tests in this section show that hydrogen detection is an actionable signal to prevent a stressed lithium-ion cell from imminently entering thermal runaway by stopping the stressor.

NCA cathode cylindrical cells

Figure 4 shows the effect of overheating cylindrical cells with 10%, 50%, and 100% SoC. The measured voltage showed no sign of first venting in any case due to the current interrupt device (CID). The pressure sensor readings spiked by 8.5, 23, and <0.1 hPa for the 10%, 50%, and 100% SoC cells, respectively. More complete environmental data are available in Figures S11–S16, and videos are available in Videos S3, S4, and S5.

The cell case temperature at first venting was between 111°C and 125°C and was not correlated with SoC. After stopping the heat source, the cell case temperature decreased for the 10% and 50% SoC cells but not for the 100% SoC cell. Earlier work has shown that higher-SoC cells have greater reactivity with electrolyte materials¹⁵ and that higher-SoC cells have more explosive failure events due to the reactivity of lithiated graphite with electrolytes,¹⁴ and this trend is also manifest at the lower-temperature phenomenon of cell venting.

The measured hydrogen concentration at venting was between 100 and 400 ppm and was not correlated with SoC. Hydrogen concentrations continued to increase slightly after



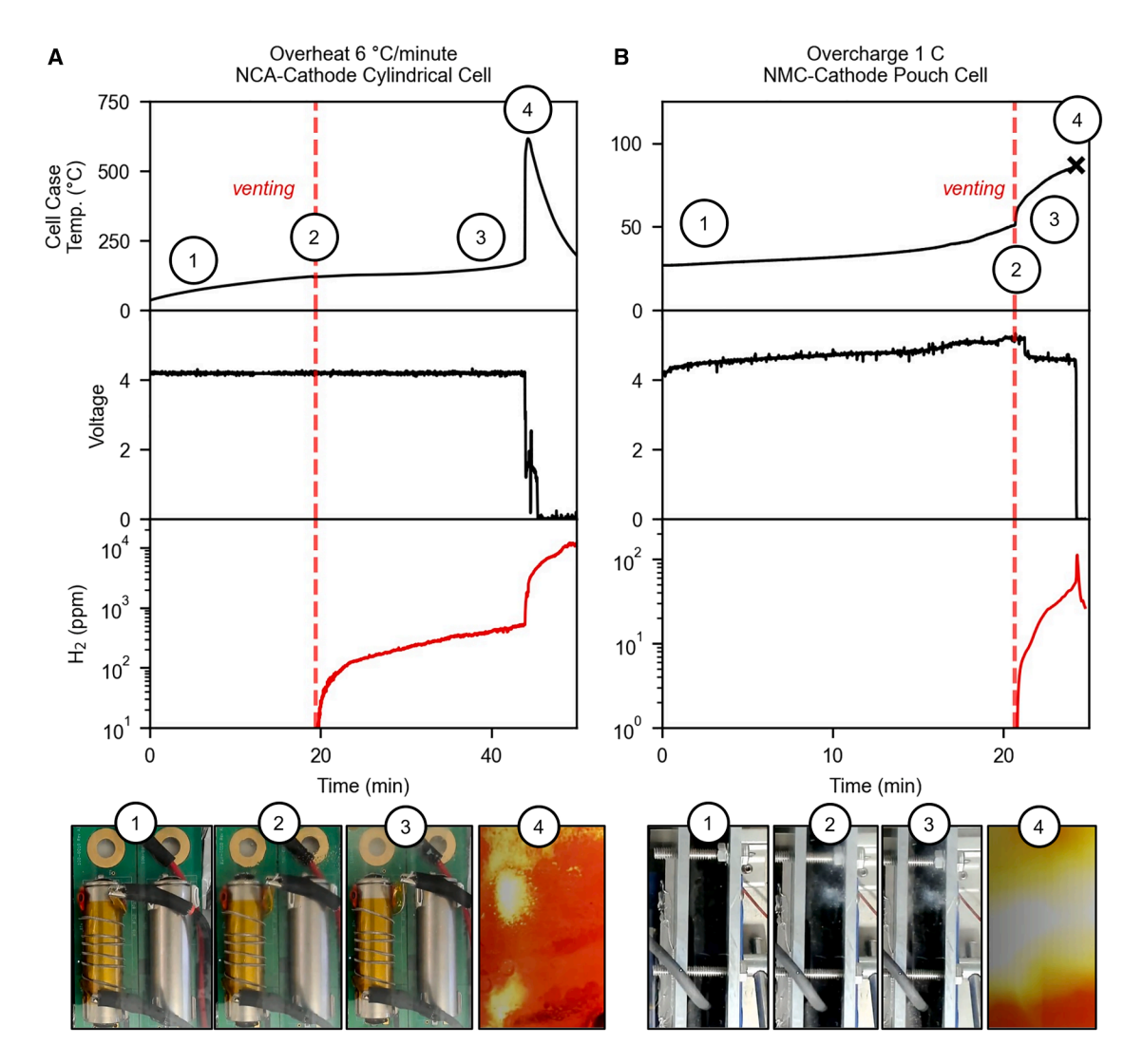


Figure 3. Hydrogen gas measurement from lithium-ion cells prior to thermal runaway

Lithium-ion cells emit hydrogen prior to thermal runaway. Video stills of each test are provided (1) at the start, (2) at first venting, (3) after first venting, and (4) at thermal runaway.

- (A) Overheating a cylindrical 2170 cell. Voltage is measured across two cells in parallel.
- (B) Overcharging a pouch cell at 1 C. \times , RTD temperature measurement was lost at thermal runaway.

stopping the heat source, similar to the behavior of the cell where the stressor was not removed, but at a much slower rate. The video of the cells did not show continued evolution of smoke after the heat was removed.

At all SoCs tested, hydrogen was detected in the vent gas, confirming its reliability as an early warning signal regardless of these cells' SoC.

NMC cathode pouch cells

Figure 5 shows thermal runaway mitigation using a hydrogen signal from NMC cathode pouch cells overheated at various states of charge and overcharged. A separate test at 100% SoC and higher heating rate of 220 W showed similar information as in Figure 5C (Figures S23 and S24). In all tests, the voltage measurements did not indicate venting, and the pressure sensor

did not detect any significant pressure changes (<0.1 hPa). More complete environmental data are available in Figures S17–S26. Videos for some tests are available as Videos S6, S7, and S8.

In overheating tests, the cell case temperature at first venting decreased with increasing SoC, suggesting that higher states of charge allow cells to build up a critical amount of gas earlier. After removing the heat source, the cell temperature continued to rise to varying degrees: less than 1°C in the 10% SoC cell, 3°C in the 50% SoC cell, 9°C in the 100% SoC cell at 110 W, and 19°C in the 100% SoC cell at 220 W.

This pattern of larger temperature increases following at higher SoC is consistent with the findings for the NCA cathode cylindrical cells, though the NMC cathode pouch cells demonstrated higher temperature increases across all SoC levels. The greater



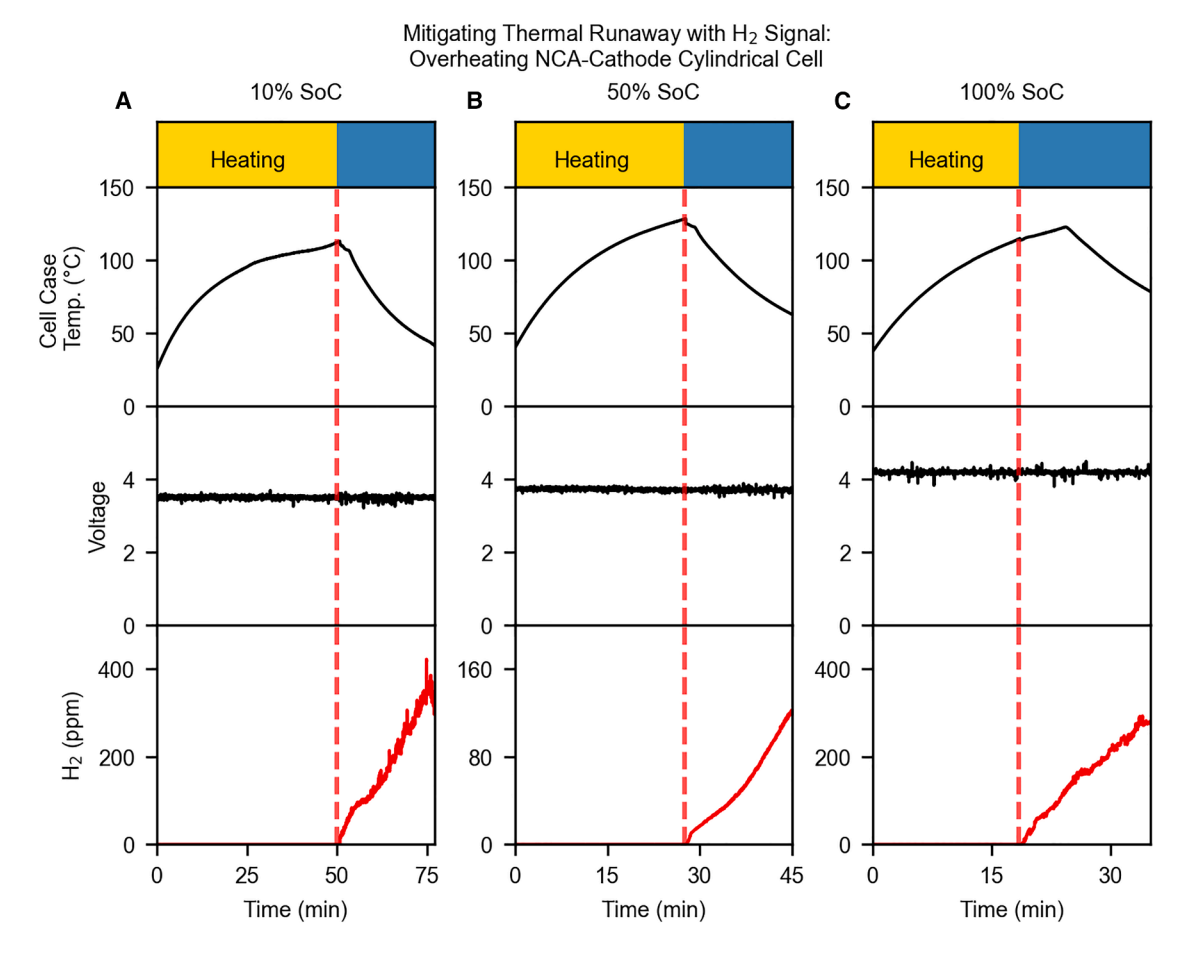


Figure 4. Thermal runaway mitigation with trace hydrogen detection in NCA cathode cells
Shown is the thermal runaway mitigation test for thermally stressed NCA cathode cylindrical lithium-ion cells at SoC of (A) 10%, (B) 50%, and (C) 100%. Red dashed lines indicate the time of the first H₂ signal.

reactivity of higher-SoC NMC cells aligns well with Rowden and Garcia-Araez, ²⁷ who reported that delithiated NMC cathodes are more reactive with the electrolyte, especially above 80% SoC. Higher-SoC cells would require more cooling than lower-SoC cells to cool to a safe temperature.

The amount of hydrogen vented showed a slight correlation with SoC. The hydrogen profile in these tests is different from that in Figure 4 due to the different abuse chamber; here, the abuse chamber is much larger, so the initial plume diffuses throughout the chamber toward a uniform value. Importantly, hydrogen was detected in each test regardless of cell SoC or heating rate, further confirming its reliability as an early warning indicator.

Figure 5D shows a pouch cell overcharged at 0.25 C until venting. The cell case temperature increased very slowly at <0.1°C/min until the cell voltage leveled off at 5.26 V, at which point the temperature began increasing more rapidly at approximately 1.1°C/min. In Jiang et al., this voltage plateau is found to indicate lithium dendrite formation. ⁴³ The cell vented when the case temperature reached 71°C, simultaneous with hydrogen detection. The cell voltage dropped approximately 30 s after venting, similar to the timing observed when a similar cell entered thermal

runaway (Figure 3B). The pressure sensor detected a modest spike of 0.3 hPa.

After ceasing overcharging, the cell case temperature continued to rise to 94°C. This was the largest temperature increase observed in any thermal runaway mitigation experiment. The temperature rose rapidly with an abrupt cell voltage drop in both Figures 5D and 3B, most likely due to accumulated lithium dendrites forming internal shorts. 43,44

Overheating LFP prismatic cell

Figure 6 shows the overheating of a prismatic cell. More complete environmental data are available at Figures S27 and S28, and a video of the test is Video S9. The cell temperature increased at approximately 2°C/min until around 55 min, when additional power was delivered to the cell to continue increasing the temperature. This cell's case temperature at venting was higher than that in any other cell tested, 142°C. The measured voltage dropped simultaneous with the venting event. The pressure sensor detected a spike of approximately 60 hPa, the largest pressure increase observed in any test.

After the venting event, the cell case temperature dropped suddenly, simultaneous with the venting rather than with cutting off power to the heater. After the initial temperature drop, the cell



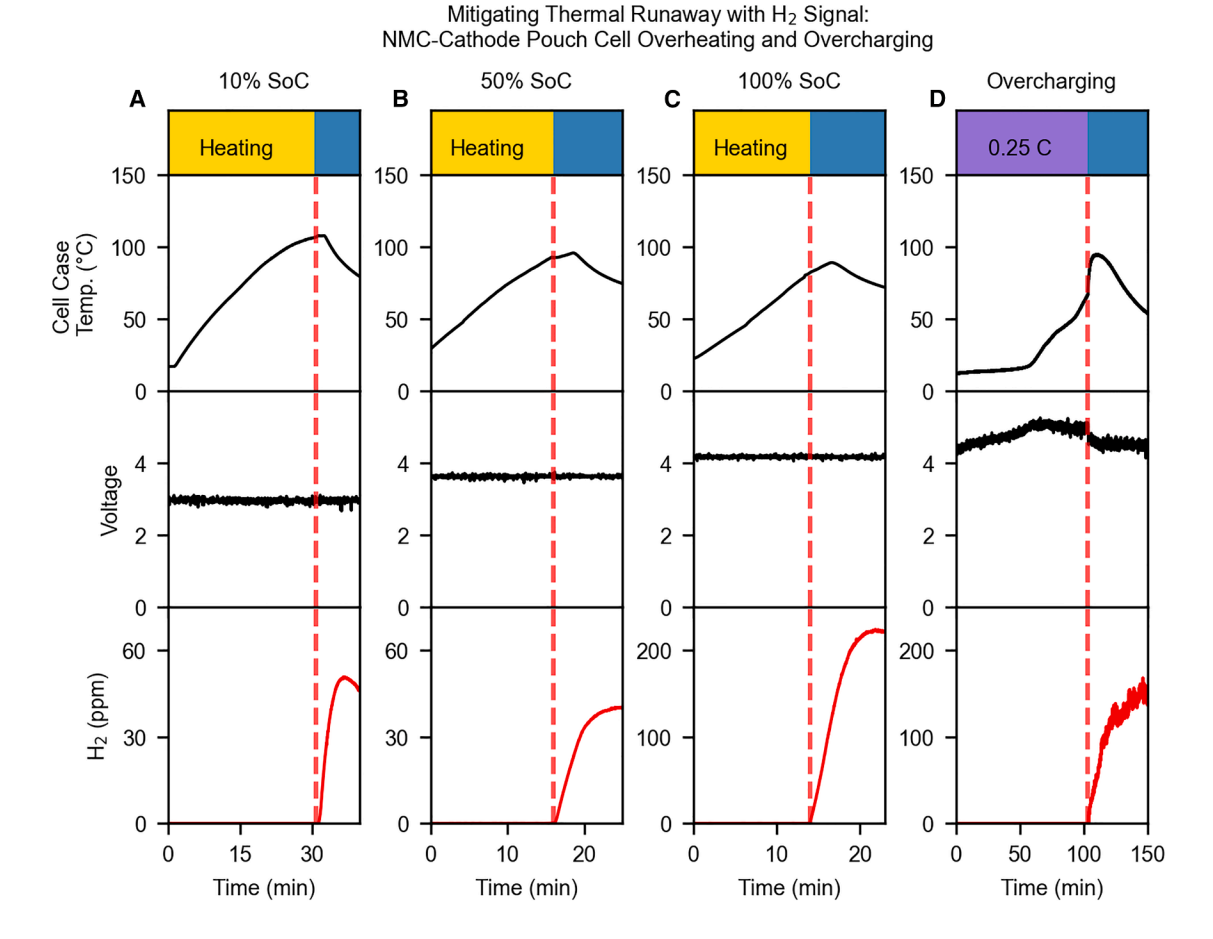


Figure 5. Thermal runaway mitigation with trace hydrogen detection in NMC cathode cells

Shown is the thermal runaway mitigation test for NMC cathode pouch lithium-ion cells thermally stressed at SoC of (A) 10%, (B) 50%, and (C) 100% and (D) overcharged. Red dashed lines indicate venting.

case temperature increased by approximately 5°C for 30 s before decreasing again. Hydrogen was detected simultaneously with the venting event. The drop in measured hydrogen concentration is attributable to the plume diffusing throughout the abuse chamber. More testing is necessary to determine how typical this behavior is of prismatic cells in general.

DISCUSSION

Thermal runaway in lithium-ion cells was mitigated by hydrogen detection using an $\rm H_2\text{-}CSFET$ across a variety of formats, chemistries, states of charge, and stressors. Mitigation tests included overheating of cylindrical NCA cathode cells, pouch NMC cathode cells, and prismatic LFP cathode cells as well as overcharging of a pouch NMC cathode cell. In experiments where the cell was pushed to thermal runaway, venting provided 23.9 min early warning from a 6°C/min overheating and 3.6 min from 1 C overcharging. Major findings from mitigation tests included the following.

 Hydrogen gas detection was a more reliable indicator of imminent thermal runaway than sensors for pressure, voltage, and cell case temperature.

- (2) Once a heating stressor was removed, temperatures in higher-SoC cells took longer to fall than in lower-SoC cells, especially in NMC cathode pouch cells.
- (3) In the overcharge test, cell temperature remained elevated for longer than in overheating tests.
- (4) SoC of overheated cylindrical NCA cathode cells did not affect the first venting temperature. SoC in overheated pouch NMC cathode cells was inversely correlated with cell venting temperature.

Within the context/application of preventing thermal runaway in lithium-ion battery packs, the underlying CSFET sensor platform can be adapted to detect other relevant battery off-gases, such as battery electrolytes and other volatile organic compounds, which could provide an additional layer of information in conjunction with trace hydrogen to identify lithium-ion cell leakage. Specifically, unique sensing layers and operating temperatures can enable selectivity for the relevant gases. Furthermore, the CSFET platform can be adapted to also detect off-gases related to newer/emerging battery chemistries, such as lithium-sulfur, where hydrogen sulfide may be released.



Mitigating Thermal Runaway with H₂ Signal: Overheating 100% SoC LFP-Cathode Prismatic Cell

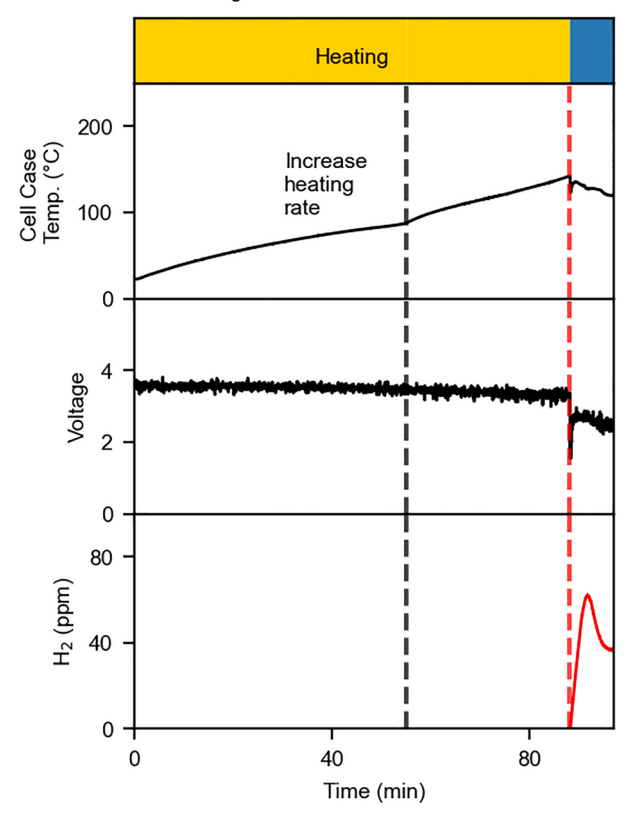


Figure 6. Thermal runaway mitigation with trace hydrogen detection in LFP cathode cells

Shown is the thermal runaway mitigation test for LFP cathode pouch lithiumion cell thermally stressed at 100% SoC.

More work is needed to understand how these results compare to cells in fully assembled commercial battery packs. The types of defects in those packs may lead to different cell temperature evolution profiles. Hydrogen gas detection provides a valuable method for detecting lithium-ion cells that may enter thermal runaway.

METHODS

Multiplexed sensor evaluation board

A custom evaluation board was used to interact with the H₂-CSFETs electronically (Figure S1). The evaluation board synchronously measures the following: H₂-CSFET sensors; ambient temperature and humidity with the Sensirion SHT-35; pressure with the ST Micro LPS22HB; cell case temperature with an RTD temperature sensor wound around the case for cylindrical cells and attached directly to the center of the case for pouch cells with the El Sensor Technologies ERTD2A102C; and cell voltage. During battery abuse tests, the evaluation board was covered and fitted with a mesh to protect board components. In larger-Ah-capacity pouch and prismatic cells, the board was also inserted into a permeable high-temperature carbon fiber sleeve (Figure S6). Diagnostic tests of the evaluation boards

following thermal runaway experiments showed that the board's components continue to perform following a thermal runaway test, though H_2 -CSFETs were discarded following thermal runaway experiments.

Additional gas sensors

A separate gas sensor, Amphenol SGX-BLD2, based on a metal oxide sensor for flammable gases, was used to corroborate venting events as well as a thermal conductivity (TC) hydrogen sensor⁴⁵ as an additional hydrogen sensor, where the TC sensor's limit of detection is roughly thousands of parts per million hydrogen. The flammable gas sensor was verified to detect a variety of battery vent gases (Figure S2). Measurements were acquired once per second.

H₂-CSFET

Hydrogen was sensed by the H $_2$ -CSFET, whose preparation using conventional silicon integrated circuit processing techniques is described elsewhere. The sensors rely on palladium's highly selective work function shift in the presence of hydrogen, which modulates the transistor's threshold voltage and, therefore, the transistor channel current. The interaction is highly specific to the molecular hydrogen H–H bond and H diffusion within Pd. Similar bonds containing hydrogen (e.g., C–H in methane or battery solvents) are not cleavable at the temperature at which we operate our sensor and are therefore not detected. The H $_2$ -CSFET hydrogen sensor is selective for all gases tested.

No other components (e.g., contacts, dielectric) are sensitive to hydrogen; when Pd is not deposited, the sensor does not respond. 41 A notable difference in this work is the use of a 10 nm palladium-sensing layer that is electrically floating rather than the $\sim\!1$ nm palladium-sensing layer used previously. The greater thickness is preferable from a consistency and manufacturability perspective. A microheater that surrounds the transistor and operates at 60°C prevents humidity and other volatiles from adsorbing to the surface while keeping the sensor response to hydrogen constant across a wide humidity range. 42 The sensor described here should be made more power efficient to prevent draining auxiliary batteries through improvements in thermal isolation to be a relevant consumer safety feature.

H₂-CSFET imaging

Cross-sectional transmission electron microscopy (TEM) shows a uniform 10 nm Pd layer (Figure S3) with no contaminants. Cross-sectional TEM analysis was performed by Covalent Metrology. Samples were coated with protective carbon. TEM lamellae were prepared by lift-out preparation technique using a Thermo Fisher Scientific (FEI) Helios UC focused ion beam-scanning electron microscope system. TEM images were acquired using a Thermo Fisher Scientific (FEI) Talos F200X G2 with a bright extreme field-emission gun source operated at 200 kV accelerating voltage and using a Gatan OneView acquisition unit. Energy dispersive spectroscopy (EDS) spectra were collected on a Thermo Fisher Scientific Super X EDS detector.

H₂-CSFET calibration and interference testing

The H_2 -CSFET sensor responses were calibrated prior to battery abuse tests by placing the evaluation board inside a custom





Table 1. Lithium-ion cells tested					
Cell	Capacity (Ah)	Voltage	Cathode	Cell size	Test volume (L)
Cylindrical	5	4.2	NCA	21 × 70 mm	3.6
Pouch	72	4.2	NMC	$23\times4\times0.4$ in	94
Prismatic	120	3.8	LFP	174 × 48 × 171 mm	94

3D-printed enclosure connected to a gas stream by a barbed fitting. A representative plot showing the raw drain current of eight CSFETs at calibration is shown in Figure S1B. Typical power consumption of the FET is $\sim 1~\mu W$. The bulk silicon microheater has a power consumption of $\sim 50~mW$, though proper isolation and duty cycling of the heated elements can significantly decrease the power consumption. 46 The logarithm of the sensor's current has a roughly linear relationship with the logarithm of the hydrogen concentration between 1 and 1,000 ppm, with experimental 41 and theoretical results showing a leveling off of the response above $\sim 5,000~ppm$ (at the current sensor temperature). 47 The relationship between sensor current and ppm reading is given by the following equation:

$$\label{eq:log2} \begin{array}{ll} \textit{Log}_2(\textit{ppm}) \ = \ \text{Log}_2(2^{\wedge}(A \ * (I + B) \ - \ 2^{\wedge}(A + B)), \\ & \text{(Equation 1)} \end{array}$$

where $Log_2(ppm)$ is the log base 2 of the hydrogen concentration in parts per million, A and B are fit parameters for the above equation, and I is the sensor current divided by a baseline value taken shortly after startup. Calculated sensor readings from an array of 4–8 H_2 -CSFETs are combined to take the median reading, given than these are not production devices, and there is some variability.

The reading from the sensor array is then filtered to guard against false positives. Readings less than 10 ppm are set to 0 ppm to avoid false positives. Readings above 25 ppm are unchanged. Readings in between are scaled as in Equation 2:

If
$$10 < ppm < 25$$
: Reading = ppm_{median} * $\left[\frac{(ppm_{median} - 10)}{(25 - 10)}\right]^2$. (Equation 2)

The above filter is used in all plots shown here except when noted otherwise in the supplemental information.

The H_2 -CSFET response is temperature compensated with a temperature sensor on the evaluation board (Figure S4) by controlling the microheaters' power in relation to the onboard temperature sensor, which enables the sensor to compensate temperature increases up to 70° C. The accuracy of the measurement between 30 and 1,000 ppm is approximately 10%. The sensor is selective to hydrogen over cell vent gases, including C_2H_4 , CO_2 , common lithium-ion cell electrolytes, and humidity (Figure S5).

Gas delivery tests for calibration, challenge, and selectivity tests were performed with pure dry air as diluent (Praxair Technology). Hydrogen gas was delivered from a 1,000 ppm tank in pure dry air. CO₂, CO, C₃H₈, and CH₄ gases were delivered

from calibration cylinders with balance of dry air. Battery solvents (dimethyl carbonate and ethyl methyl carbonate) were delivered by flowing a dry diluent stream that passed through the battery solvent liquid. Co-feeding experiments (as in Figure S5) were conducted by mixing a hydrogen gas stream with a stream of the interferant or with a stream from a bubbled solvent. Typical gas flow rates were approximately 1,000 standard cubic centimeters per minute. Gas delivery was controlled by mass flow controllers (Alicat Scientific). The H₂-CSFET sensor responses were calibrated prior to battery abuse tests by placing the evaluation board inside a custom 3D-printed enclosure connected to a gas stream by a barbed fitting.

Stressing Li-ion cells

A battery abuse chamber was constructed to house the cells, evaluation board, and corroborating sensors (Figure S6). The chamber walls are made with an exoskeleton of reinforced aluminum and include polycarbonate windows for lighting and video capture. The free chamber internal volume is 3.6 L in the cylindrical cell tests and 94 L in the pouch and prismatic cell tests. A smaller chamber was used for the cylindrical cells to achieve a more uniform ratio of battery size to chamber volume. The sensors are 85 mm from the nearest cell when testing cylindrical cells and 75 mm from the cell when testing pouch and prismatic cells. Ambient temperature was ~25°C and increased <10°C prior to all first venting events. The tests were performed in atmospheric air. The chamber was sealed with a monostable venting port during battery abuse tests. Baseline measurements were recorded for at least 1 h prior to applying a stressor. The chamber was opened, and reaction products were vented following abuse tests. Between battery abuse tests, the chamber was cleaned to remove any vent products.

Three different cells of three different chemistries, sizes, and formats were tested in this study and are summarized in Table 1. Fresh (non-aged) cells were used in all tests. Cells were stored at 25°C between arrival at the test facility and testing. Cells were charged to full capacity and then load tested to a lower voltage to determine the capacity of each cell. Cells were then recharged and subsequently discharged to a 10%, 50%, or 100% SoC as defined by the measured capacity. In each test with cylindrical cells, two cells were placed in parallel to simulate the voltage signal that would be read by a voltage sensor for a pack of cells.

Overheating tests

In overheating tests of cylindrical cells, two cells were placed in parallel. Nichrome wire was wrapped around one of the cells as a heat source at 12.5 W for an initial heating rate of $\sim\!6^\circ\text{C/min}$. Cylindrical cells contain a safety device known as a CID, which prevents overcharging. When a single cell is stressed, pressure inside the cell increases until the CID activates, and the voltage across the stressed cell's electrodes drops. In practice, cylindrical cells are massively in parallel, which prevents a measured voltage from identifying a problem with the cell.

In overheating tests of pouch cells, a 3D-printed heating pad was used as heat source, with a welding blanket for insulation. Power supply was set to 110 or 220 W for initial heating rates of $\sim\!4^{\circ}\text{C}$ and 8°C/min , respectively. In overheating tests of the

Cell Reports Physical Science

Article



prismatic cell, heating was done with two 120 \times 120 mm silicone heater pads, one on each side of the cell, connected in series. Power supply was set to 115 W and then 230 W for heating rates of 2.1 $^{\circ}$ C-2.6 $^{\circ}$ C/min.

In mitigation tests, external heating was stopped as soon as hydrogen was detected by the $\rm H_2\text{-}CSFET$ sensor to simulate a corrective action being taken in response to gas detection.

Overcharging tests

In the overcharging test that ended in thermal runaway, the power source was a Sorensen XG 1700. The supply was limited to 9.0 V and 73.5 A with a 1 C charging rate starting at $\sim\!4.2$ V, as seen by the cell. In the overcharge test where thermal runaway was mitigated, the power source was a Riden RD6018 (maximum outputs: 18.1 A, 48 V). The supply was limited to 7.2 V and 18.0 A, resulting in a 0.25 C charging rate starting at $\sim\!4.2$ V as seen by the cell. The second power supply was used because it could be controlled to automatically turn off when hydrogen was detected.

A summary of all tests is provided in Table S1.

RESOURCE AVAILABILITY

Lead contact

Requests for further information and resources should be directed to and will be fulfilled by the lead contact, Hossain M. Fahad (fahad@serinuslabs.com).

Materials availability

This study did not generate new unique reagents.

Data and code availability

- Battery abuse data and videos and representative calibration and sensor selectivity data have been deposited at the Figshare repository with DOI:https://doi.org/10.6084/m9.figshare.28677122.v2. They are publicly available as of the date of publication. Battery abuse data include measured hydrogen, cell voltage, cell case temperature, ambient pressure, ambient humidity, ambient temperature, metal-oxide gas sensor, and TC hydrogen sensor. Files are labeled according to their respective figure.
- This paper does not report original code.
- Any additional information required to reanalyze the data reported in this
 paper is available from the lead contact upon request.

ACKNOWLEDGMENTS

This material is based upon work supported by the U.S. National Science Foundation under award No. 2112273. Any opinions, findings, and conclusions or recommendations expressed in this material are those of the author(s) and do not necessarily reflect the views of the U.S. National Science Foundation.

AUTHOR CONTRIBUTIONS

Conceptualization, G.C. and H.M.F.; formal analysis, D.W.G.; investigation, G. C. and D.W.G.; methodology, G.C. and H.M.F.; resources, G.C., D.W.G., and T.N.; writing – original draft, D.W.G.; writing – review and editing, D.W.G., H.M. F., G.C., A.J., and T.N.; project administration, H.M.F.; supervision, H.M.F.; funding acquisition, H.M.F.

DECLARATION OF INTERESTS

D.W.G., G.C., T.N., and H.M.F. declare competing financial interests as employees of Serinus Labs, Inc. All authors declare competing financial interests

in equity on shares of Serinus Labs, Inc. G.C., A.J., and H.M.F. declare competing interest as co-founders of Serinus Labs, Inc. The following published patents, assigned jointly to Serinus Labs, Inc. and The Regents of the University of California, may have their value affected by this publication: US11626626B2 (inventors: H.M.F., and A. J.), US20230244200A1 (inventors: G.C., H.M.F., and A.J.), and WO2024215302A1 (inventors: G.C., H.M.F., and A.J.). An invention disclosure on this work has been filed with Serinus Labs, Inc. and the University of California, Berkeley.

SUPPLEMENTAL INFORMATION

Supplemental information can be found online at https://doi.org/10.1016/j.xcrp.2025.102859.

Received: April 11, 2025 Revised: July 1, 2025 Accepted: August 29, 2025 Published: September 25, 2025

REFERENCES

- Golubkov, A.W., Planteu, R., Krohn, P., Rasch, B., Brunnsteiner, B., Thaler, A., and Hacker, V. (2018). Thermal runaway of large automotive Li-ion batteries. RSC Adv. 8, 40172–40186. https://doi.org/10.1039/ C8RA06458J.
- Qiu, Y., and Jiang, F. (2022). A review on passive and active strategies of enhancing the safety of lithium-ion batteries. Int. J. Heat Mass Transf. 184, 122288. https://doi.org/10.1016/j.ijheatmasstransfer.2021.122288.
- Feng, X., Ouyang, M., Liu, X., Lu, L., Xia, Y., and He, X. (2018). Thermal runaway mechanism of lithium ion battery for electric vehicles: A review. Energy Storage Mater. 10, 246–267. https://doi.org/10.1016/j.ensm. 2017.05.013.
- Li, J., Li, Y., and Zeng, W. (2024). Gas sensing technology as the key to safety warning of lithium-ion battery: Recent advance. Sens. Actuators A Phys. 365, 114890. https://doi.org/10.1016/j.sna.2023.114890.
- Galushkin, N.E., Yazvinskaya, N.N., and Galushkin, D.N. (2019). Mechanism of Gases Generation during Lithium-Ion Batteries Cycling. J. Electrochem. Soc. 166, A897–A908. https://doi.org/10.1149/2.0041906jes.
- Galushkin, N.E., Yazvinskaya, N.N., and Galushkin, D.N. (2018). Mechanism of Thermal Runaway in Lithium-Ion Cells. J. Electrochem. Soc. 165, A1303–A1308. https://doi.org/10.1149/2.0611807jes.
- Krisher, T. (2022). NHTSA Opens Investigation into Electric Vehicle Batteries (Detroit Free Press).
- Larsson, F., and Mellander, B.-E. (2014). Abuse by External Heating, Overcharge and Short Circuiting of Commercial Lithium-Ion Battery Cells.
 Electrochem. Soc. 161, A1611–A1617. https://doi.org/10.1149/2.0311410jes.
- Liu, P., Liu, C., Yang, K., Zhang, M., Gao, F., Mao, B., Li, H., Duan, Q., and Wang, Q. (2020). Thermal runaway and fire behaviors of lithium iron phosphate battery induced by over heating. J. Energy Storage 31, 101714. https://doi.org/10.1016/j.est.2020.101714.
- Essl, C., Seifert, L., Rabe, M., and Fuchs, A. (2021). Early detection of failing automotive batteries using gas sensors. Batteries 7, 25. https:// doi.org/10.3390/batteries7020025.
- Essl, C., Golubkov, A., Thaler, A., and Fuchs, A. (2020). Comparing Different Thermal Runaway Triggers for Automotive Lithium-Ion Batteries. ECS Meet. Abstr. 436. https://doi.org/10.1149/ma2020-012436mtgabs.
- Preger, Y., Torres-Castro, L., Rauhala, T., and Jeevarajan, J. (2022).
 Perspective—On the safety of aged lithium-ion batteries. J. Electrochem. Soc. 169, 030507. https://doi.org/10.1149/1945-7111/ac53cc.
- Belharouak, I., Koenig, G.M., Tan, T., Yumoto, H., Ota, N., and Amine, K. (2012). Performance Degradation and Gassing of Li4Ti5O12/LiMn2O4 Lithium-Ion Cells. J. Electrochem. Soc. 159, A1165–A1170. https://doi.org/10.1149/2.013208jes.



Cell Reports Physical Science Article

- Spinner, N.S., Hinnant, K.M., Tuttle, S.G., and Rose-Pehrsson, S.L. (2016).
 Lithium-Ion Battery Failure: Effects of State of Charge and Packing Configuration.
 Navy Technology Center for Safety and Survivability, Chemistry Division. https://apps.dtic.mil/sti/pdfs/AD1016095.pdf
- Gachot, G., Grugeon, S., Eshetu, G.G., Mathiron, D., Ribière, P., Armand, M., and Laruelle, S. (2012). Thermal behaviour of the lithiated-graphite/ electrolyte interface through GC/MS analysis. Electrochim. Acta 83, 402–409. https://doi.org/10.1016/j.electacta.2012.08.016.
- UNECE (2018). Global Technical Regulation No. 20: Electric Vehicle Safety (EVS). ECE/TRANS/180/Add.20 (Geneva: United Nations Economic Commission for Europe). https://unece.org/fileadmin/DAM/trans/main/wp29/ wp29wgs/wp29gen/wp29registry/ECE-TRANS-180a20e.pdf.
- (2025). Federal Motor Vehicle Safety Standards; FMVSS No. 305a Electric-Powered Vehicles: Electric Powertrain Integrity, Global Technical Regulation No. 20. Fed. Regist. 90, 9609–9610.
- Lyu, N., Shi, S., Lu, H., Song, Y., Jiang, X., and Jin, Y. (2023). Hydrogen gas diffusion behavior under fault conditions and detector installation optimization of electric vehicles. Process Saf. Environ. Prot. 175, 565–574. https://doi.org/10.1016/j.psep.2023.05.075.
- Koch, S., Birke, K., and Kuhn, R. (2018). Fast thermal runaway detection for lithium-ion cells in large scale traction batteries. Batteries 4, 16. https://doi.org/10.3390/batteries4020016.
- Torres-Castro, L., Bates, A.M., Johnson, N.B., Quintana, G., and Gray, L. (2024). Early Detection of Li-Ion Battery Thermal Runaway Using Commercial Diagnostic Technologies. J. Electrochem. Soc. 171, 020520. https://doi.org/10.1149/1945-7111/ad2440.
- Shi, S., Lyu, N., Jiang, X., Song, Y., Lu, H., and Jin, Y. (2023). Hydrogen gas diffusion behavior and detector installation optimization of lithium ion battery energy-storage cabin. J. Energy Storage 67, 107510. https://doi.org/ 10.1016/j.est.2023.107510.
- Huang, W., Feng, X., Pan, Y., Jin, C., Sun, J., Yao, J., Wang, H., Xu, C., Jiang, F., and Ouyang, M. (2023). Early warning of battery failure based on venting signal. J. Energy Storage 59, 106536. https://doi.org/10. 1016/j.est.2022.106536.
- Wang, Z., Zhu, L., Liu, J., Wang, J., and Yan, W. (2022). Gas Sensing Technology for the Detection and Early Warning of Battery Thermal Runaway: A Review. Energy Fuels 36, 6038–6057. https://doi.org/10.1021/acs.energyfuels.2c01121.
- Hill, D., Gully, B., Agarwal, A., Nourai, A., Thrun, L., Swartz, S., Koslowske, M., Cummings, S., Butkowski, J., and Moore, B. (2013). Detection of off gassing from Li-ion batteries. In 2013 IEEE Energytech (IEEE), pp. 1–6. https://doi.org/10.1109/EnergyTech.2013.6645307.
- Nilsson, E.J.K., and Ahlberg Tidblad, A. (2024). Gas Emissions from Lithium-Ion Batteries: A Review of Experimental Results and Methodologies. Batteries 10, 443. https://doi.org/10.3390/batteries10120443.
- Cui, Y., Shi, D., Wang, Z., Mou, L., Ou, M., Fan, T., Bi, S., Zhang, X., Yu, Z., and Fang, Y. (2023). Thermal Runaway Early Warning and Risk Estimation Based on Gas Production Characteristics of Different Types of Lithium-Ion Batteries. Batteries 9, 438. https://doi.org/10.3390/batteries9090438.
- Rowden, B., and Garcia-Araez, N. (2020). A review of gas evolution in lithium ion batteries. Energy Rep. 6, 10–18. https://doi.org/10.1016/j. egyr.2020.02.022.
- Jung, R., Metzger, M., Maglia, F., Stinner, C., and Gasteiger, H.A. (2017).
 Oxygen Release and Its Effect on the Cycling Stability of LiNixMnyCozO2 (NMC) Cathode Materials for Li-Ion Batteries. J. Electrochem. Soc. 164, A1361–A1377. https://doi.org/10.1149/2.0021707jes.
- Baird, A.R., Archibald, E.J., Marr, K.C., and Ezekoye, O.A. (2020). Explosion hazards from lithium-ion battery vent gas. J. Power Sources 446, 227257. https://doi.org/10.1016/j.jpowsour.2019.227257.
- Jin, Y., Zheng, Z., Wei, D., Jiang, X., Lu, H., Sun, L., Tao, F., Guo, D., Liu, Y., Gao, J., and Cui, Y. (2020). Detection of Micro-Scale Li Dendrite via H2 Gas Capture for Early Safety Warning. Joule 4, 1714–1729. https://doi. org/10.1016/j.joule.2020.05.016.

- Agubra, V., and Fergus, J. (2013). Lithium ion battery anode aging mechanisms. Materials 6, 1310–1325. https://doi.org/10.3390/ma6041310.
- Chalamala, B.B.R., Rosewater, D., Preger, Y., Wittman, R., Lamb, J., and Kashiwakura, A. (2021). Grid-Scale Energy Storage Systems. Annu. Rev. Chem. Biomol. Eng. 12, 19–28. https://doi.org/10.1146/annurev-chembioeng-101220-102204.
- Metzger, M., Strehle, B., Solchenbach, S., and Gasteiger, H.A. (2016). Origin of H2 Evolution in LIBs: H2O Reduction vs. Electrolyte Oxidation. J. Electrochem. Soc. 163, A798–A809. https://doi.org/10.1149/2.1151605jes.
- Lamb, J., Orendorff, C.J., Roth, E.P., and Langendorf, J. (2015). Studies on the Thermal Breakdown of Common Li-Ion Battery Electrolyte Components. J. Electrochem. Soc. 162, A2131–A2135. https://doi.org/10.1149/ 2.0651510jes.
- Nie, B., Dong, Y., and Chang, L. (2024). The evolution of thermal runaway parameters of lithium-ion batteries under different abuse conditions: A review.
 J. Energy Storage 96, 112624. https://doi.org/10.1016/j.est.2024.112624.
- Wei, G., Huang, R., Zhang, G., Jiang, B., Zhu, J., Guo, Y., Han, G., Wei, X., and Dai, H. (2023). A comprehensive insight into the thermal runaway issues in the view of lithium-ion battery intrinsic safety performance and venting gas explosion hazards. Appl. Energy 349, 121651. https://doi. org/10.1016/j.apenergy.2023.121651.
- Xueqin, Y., and Lei, Y. (2021). Exploration of the cause of hydrogen generation in NCM lithium-ion batteries. Energy Storage Sci. Technol. 10, 1693–1698. https://doi.org/10.19799/j.cnki.2095-4239.2020.0222.
- Tsiouvaras, N., Meini, S., Buchberger, I., and Gasteiger, H.A. (2013). A novel on-line mass spectrometer design for the study of multiple charging and discharging of secondary batteries. J. Electrochem. Soc. 160, A471– A479. https://doi.org/10.1149/2.042303jes.
- Geng, L., Wood, D.L., Lewis, S.A., Connatser, R.M., Li, M., Jafta, C.J., and Belharouak, I. (2020). High accuracy in-situ direct gas analysis of Li-ion batteries. J. Power Sources 466, 228211. https://doi.org/10.1016/j.jpowsour.2020.228211.
- Koch, S., Fill, A., and Birke, K.P. (2018). Comprehensive gas analysis on large scale automotive lithium-ion cells in thermal runaway. J. Power Sources 398, 106–112. https://doi.org/10.1016/j.jpowsour.2018.07.051.
- Fahad, H.M., Gupta, N., Han, R., Desai, S.B., and Javey, A. (2018). Highly Sensitive Bulk Silicon Chemical Sensors with Sub-5 nm Thin Charge Inversion Layers. ACS Nano 12, 2948–2954. https://doi.org/10.1021/acsnano. 8b00580.
- Gupta, N., Fahad, H.M., Amani, M., Song, X., Scott, M., and Javey, A. (2019). Elimination of response to relative humidity changes in chemical-sensitive field-effect transistors. ACS Sens. 4, 1857–1863. https://doi.org/10.1021/acssensors.9b00637.
- Jiang, L., Luo, Z., Wu, T., Shao, L., Sun, J., Liu, C., Li, G., Cao, K., and Wang,
 Q. (2019). Overcharge Behavior and Early Warning Analysis of LiNio.5-Coo.2Mno.3O2/C Lithium-Ion Battery with High Capacity. J. Electrochem.
 Soc. 166, A1055–A1062. https://doi.org/10.1149/2.0571906jes.
- Aryanfar, A., Brooks, D., Merinov, B.V., Goddard, W.A., Colussi, A.J., and Hoffmann, M.R. (2014). Dynamics of lithium dendrite growth and inhibition: Pulse charging experiments and monte carlo calculations. J. Phys. Chem. Lett. 5, 1721–1726. https://doi.org/10.1021/jz500207a.
- (2022). Hydrogen and Battery Leakage Detection Sensor SGX-BLD2. In Datasheet DS-0460-SGX-BLD2, Issue 6. SGX Europe Sp. z o.o. (Katowice, Poland).
- Harley-Trochimczyk, A., Chang, J., Zhou, Q., Dong, J., Pham, T., Worsley, M.A., Maboudian, R., Zettl, A., and Mickelson, W. (2015). Catalytic hydrogen sensing using microheated platinum nanoparticle-loaded graphene aerogel. Sens. Actuators B Chem. 206, 399–406. https://doi.org/ 10.1016/j.snb.2014.09.057.
- Hughes, R.C., Schubert, W.K., and Buss, R.J. (1995). Solid-State Hydrogen Sensors Using Palladium-Nickel Alloys: Effect of Alloy Composition on Sensor Response. J. Electrochem. Soc. 142, 249–254. https://doi.org/10.1149/1.2043887.